Abdominal Radiology

Published online: 18 September 2018

Abdom Radiol (2019) 44:642–651
https://doi.org/10.1007/s00261-018-1777-8

Renal solitary fibrous tumor/hemangiopericytoma: computed tomography findings and clinicopathologic features

Xiaoping Yi,[1,2,3,4] Jing Wang,[1] Youming zhang,[1] Zixin Wang,[1] Zinan Zhang,[1] Guanghui Gong,[5] Longfei Liu,[6] Wang Xiang,[7] Weihua Liao,[1] Chishing Zee,[4] and Bihong T. Chen[3]

[1]Department of Radiology, Xiangya Hospital, Central South University, No. 87 Xiangya Road, Changsha 410008, People's Republic of China
[2]Postdoctoral Research Workstation of Pathology and Pathophysiology, Basic Medical Sciences, Xiangya Hospital, Central South University, Changsha, People's Republic of China
[3]Department of Diagnostic Radiology, City of Hope National Medical Center, Duarte, CA, USA
[4]Department of Radiology, Keck Medical Center of USC, Los Angeles, CA, USA
[5]Department of Pathology, Xiangya Hospital, Central South University, Changsha, People's Republic of China
[6]Department of Urology, Xiangya Hospital, Central South University, Changsha, People's Republic of China
[7]Department of Diagnostic Radiology, the Affiliated Cancer Hospital of Xiangya School of Medicine, Central South University, Changsha, People's Republic of China

Abstract

Purpose: To retrospectively characterize the clinical, pathological, and computed tomography (CT) findings of renal solitary fibrous tumor/hemangiopericytoma (rSFT/HPC).

Methods: Twelve patients with rSFT/HPCs were enrolled. The CT findings and clinicopathological features were retrospectively reviewed.

Results: This study included six male and six female patients (median age: 47; age range: 20–82 years). Eight benign (grade I) and four malignant (grade III) rSFT/HPCs were identified. Of the 12 lesions, 10 were in the renal sinus near the renal pelvis, while two replaced the whole kidney. Five lesions were well-defined, five were partially ill-defined, and two were ill-defined. Mild (5/12) and intermediate (1/12) hydronephrosis was observed. On the unenhanced CT images, ten tumors showed slightly higher density when compared to the normal renal parenchyma, and two masses were isodense to hypodense. After intravenous contrast medium injection, three enhancement patterns were observed, including "prolonged enhancement" (PE) (6/12), "gradual enhancement" (4/12), and "early washout" (2/12). A central fibrous scar was found in five patients. Compared to the grade I lesions, the grade III rSFT/HPC lesions tended to be larger (maximal diameter > 10 cm) and more heterogeneous with a higher incidence of the PE pattern.

Conclusions: We have shown that rSFT/HPCs usually arise from the renal sinus, and present as lobulated, slightly hyperdense, gradually enhancing soft tissue masses. CT findings, including large size, heterogeneity, and the PE pattern, may assist in the pre-operative identification of malignant grade III rSFT/HPCs.

Key words: Kidney—Computed tomography—Solitary fibrous tumor—Hemangiopericytoma—Pathology—Renal cell carcinoma

Solitary fibrous tumors (SFTs) and hemangiopericytomas (HPCs), initially characterized by Klemperer and Rabin in 1931, are rare spindle cell neoplasms originating from mesenchymal tissue [1–3]. Recently, overwhelming evidence demonstrated that SFTs and HPCs show completely overlapping morphologic and genetic features

Electronic supplementary material The online version of this article (https://doi.org/10.1007/s00261-018-1777-8) contains supplementary material, which is available to authorized users.

Correspondence to: Xiaoping Yi; *email:* yixiaoping@csu.edu.cn; Youming zhang; *email:* zhangym0820@csu.edu.cn

[3, 4], and pathologists tend to classify these two tumors into one category [1, 2]. SFT/HPCs can manifest anywhere in the body, but they are extremely rare in the kidney [4–9]. Since 1977, only approximately 74 renal SFT/HPC (rSFT/HPC) cases have been reported in the English-language literature, including 12 malignant cases, and all were in case reports [10–12] (Online Resource 1 lists the case details). In clinical practice, it is easy to misdiagnose rSFT/HPCs as other tumors arising in the kidney, such as renal cell carcinoma (RCC), or as retroperitoneal tumors [9–11, 13, 14]. Therefore, accurate pre-operative identification of rSFT/HPCs is important so clinicians can avoid extensive surgery, especially radical nephrectomy and regional lymph node dissection. However, the accurate pre-operative characterization of indeterminate rSFT/HPCs remains a challenge for clinicians.

Although aspiration biopsy may be an effective method for pre-operative identification of indeterminate renal tumors [15], its clinical application is limited due to its invasive nature, the relatively high misdiagnosis rate due to size limitations and the high risk of needle tract metastasis [15]. Computed tomography (CT), as a non-invasive imaging method widely used in the abdomen, could provide valuable diagnostic information to assist clinicians and radiologists in making a reasonable diagnostic decision when an indeterminate renal tumor is encountered. Unfortunately, although some clinicopathological information has been reported for rSFT/HPCs, only limited CT characteristics of rSFT/HPCs have been presented for sporadic cases [8, 15, 16]. Therefore, the CT characteristics of rSFT/HPCs are still largely unknown.

In the present study, we retrospectively reviewed the CT characteristics and the clinicopathological features of 12 surgically and pathologically confirmed rSFT/HPCs. We present some novel and useful CT findings, which may assist in improving the pre-operative identification accuracy of rSFT/HPCs in clinical practice.

Materials and methods

Patients

This retrospective study was approved by the Ethics Committee and Institutional Review Board in Xiangya Hospital of Central South University, P. R. China (IRB No. 201612639), and the requirement for informed consent was waived for this study. The study was performed in accordance with the ethical standards as laid down in the 1964 Declaration of Helsinki and its later amendments.

Complete clinical, imaging, and pathological data of the 12 patients with rSFT/HPCs treated in our hospital from March 2010 to February 2017 were retrieved from the database and medical records. All rSFT/HPCs were confirmed surgically and pathologically.

CT imaging acquisition and analysis

The CT scans were performed in our hospital following standard scanning protocols. Two radiologists who specialize in abdominal imaging independently evaluated the CT features of the rSFT/HPCs. The investigators were blinded to the clinical findings and to the histopathologic results and inconsistencies were resolved via consensus. Measurement of CT attenuation values was performed with a previously reported method [17]. Three time-course enhancement patterns, including early wash-out (EW), gradual enhancement (GE) (Fig. 1), and prolonged enhancement (PE), were defined based on criteria reported in previous studies [17]. Additionally, a gradual wash-out (GW) pattern was defined when the CT value of the subsequent phase was reduced to less than 20 Hounsfield units. Details are in the Online Resource 2 and Online Resource 3.

Pathological analysis

All pathology samples from the 12 rSFT/HPCs, including the hematoxylin/eosin and immunohistochemistry (IHC) sections, were re-analyzed independently by two experienced pathologists. The findings were recorded by consensus. Additional sections were obtained from the corresponding paraffin blocks when needed. IHC analysis included expression of CD34, CD99, Ki-67, Vimentin, B cell lymphoma 2 (Bcl-2), epithelial membrane antigen (EMA), and S100. In addition, nuclear atypia, cellular pleomorphism, hyper-cellularity, necrosis, and high mitotic rate ($>$ 4 mitoses/10 HPF) were also assessed to evaluate the atypical or malignant features of the rSFT/HPCs.

Follow-up

The follow-up period was defined as the period from the first day of treatment to the day of death or the date of the last follow-up examination.

Statistics

Statistical analysis was performed using SPSS 22.0 (IBM Corp., Armonk, NY, USA). For the quantitative features, the Wilcoxon rank-sum test was used. For the qualitative features, the χ^2 test or Fisher's exact test were used to test for differences between groups. A *P*-value of less than 0.05 was considered statistically significant.

Results

Clinical data

The study group consisted of six men and six women with a median age of 47 years (age range 20–82 years). The clinical symptoms were diverse and non-specific,

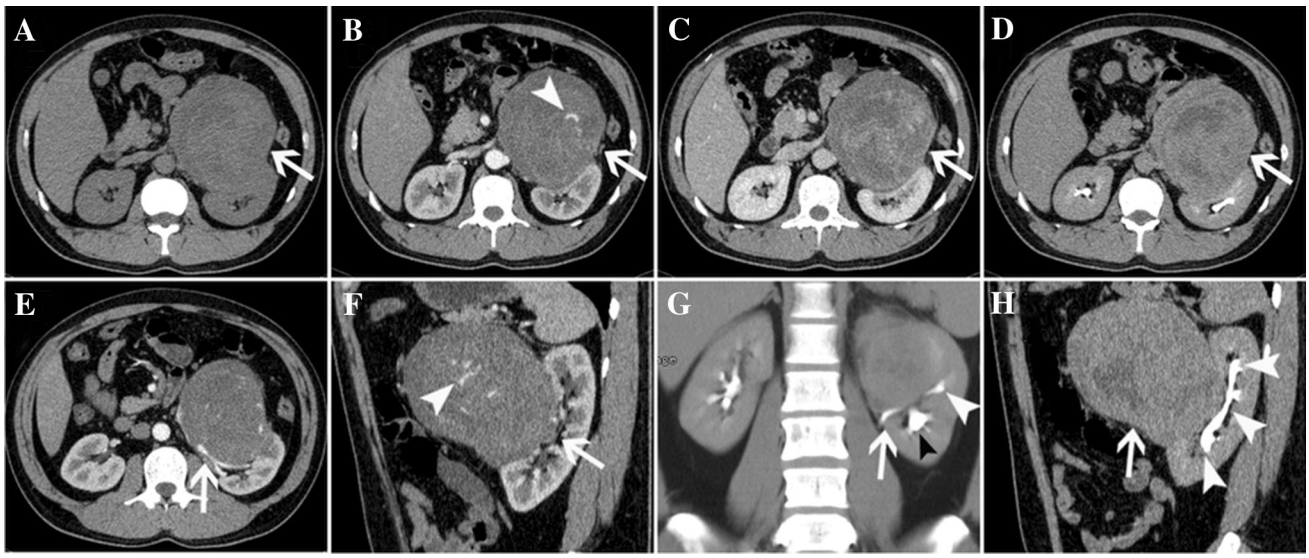

Fig. 1. A 37-year-old male patient (case 6) with a left renal hilum/parapelvic rSFT/HPC (grade III) was admitted because of left back pain. Panels **A**–**D** showing CT images with four phases: an unenhanced scan (UE), along with the corticomedullary (CM), nephrographic (N), and excretory (E) phases. Lesions are shown (arrows). Transverse (E) and sagittal (F) images show the tumor (arrows) located in the renal pelvis. Panels **B** and **F** depict prominent intratumoral vasculature (arrowheads). Panel **F** (arrowhead) shows displacement of the renal vessels around the tumor without obvious gross invasion. Panels **G** and **H** show the tumor (arrows) compressing the renal pelvis and calyces, resulting in slight hydronephrosis. The slightly dilated calices (**G**, black arrowhead), non-dilated calices (**G**, **H**, white arrowheads), and normal upper ureter (**G**, arrow) are shown. Panel **H** (arrowhead) shows the lobulated tumor bulging into the renal sinus.

including back pain (58.3%, 7/12), abdominal pain (16.7%, 2/12), hematuria (16.7%, 2/12), and non-specific incidental symptoms (25.0%, 3/12). The duration of symptoms varied from 10 days to 2 years. Abnormal findings in the routine laboratory tests included urinary occult blood (58.3%, 7/12) and urine protein (16.7%, 2/12). Pre-operative metastatic disease was observed in one patient. All tumors in this study were pre-operatively misdiagnosed as RCCs. The details are presented in Table 1.

Imaging findings

The detailed CT findings for the 12 rSFT/HPCs are shown in Table 2. All patients presented with unilateral, solitary renal tumors, with eight (66.7%) lesions involving the left kidney, and four involving the right kidney (33.3%). The lesions had an average maximal diameter of 7.42 ± 4.71 cm (range: 2.10–16.48 cm), and, to varying degrees, they appeared as lobulated shapes (Figs. 1, 2, 3, Online Resource 4-5). In two (16.7%) patients, the right kidney was replaced by the tumor. The remaining 10 lesions were in the renal sinus near the renal pelvis (83.3%), including two in the upper pole level (16.7%), one in the midpolar level (8.3%), and seven around the renal hilum (58.3%). The growth patterns of the tumors were divided into three subtypes: intrapelvic, extra-renal exophytic, and intra-renal infiltrative growth (Fig. 3). No significant hydronephrosis was found, even in patients with large tumors (maximal diameter exceeding 10 cm), and mild (41.7%, 5/12) (Fig. 1G, H) and intermediate (8.3%, 1/12) hydronephrosis was identified (Table 2).

Of the 12 masses, five (41.7%) were well-defined, five (41.7%) were partially ill-defined, and the remaining two (16.6%) were ill-defined. Seventy-five percent (9/12) of the tumors demonstrated a partially or totally ill-defined boundary, and only three (25.0%) tumors had a totally sharp boundary.

On the unenhanced CT images, 10 tumors showed a slightly hyperdense appearance with a pseudocapsule, when compared to the normal renal parenchyma, (Fig. 1, Online Resource 4–5) and the other two masses presented with an isodense/hypodense appearance (Fig. 2). All 12 masses showed a black-and-white alternating appearance in typical imaging slices (Fig. 1A).

After the intravenous administration of contrast agent, 91.7% (11/12) of the tumors demonstrated heterogeneous enhancement, with variable, non-enhancing areas of necrosis in the center. One (8.3%) tumor showed homogeneous enhancement. Calcifications were observed for two (16.7%) patients. Hemorrhage was identified in only one (8.3%) patient. Half of the tumors (6/12) contained obvious intratumoral vasculature; many

Table 1. Clinical data for the 12 renal solitary fibrous tumor/hemangiopericytomas (rSFT/HPCs)

Case no.	Gender	Age (y)	Presenting symptoms	Duration	UBC	UP	Misdiagnosed as	TN	Pre-met	Surgery	Follow-up (month)	Post-operative Rec/Met (time)	Survival status
1	F[a]	51	None, found incidentally	12 days	−	−	RCC	Single	No	Lap/NSS	77	None	Alive
2	F	60	Lower abdominal pain	13 days	−	−	RCC	Single	No	Lap/Nep	66	None	Alive
3	F	35	Right back pain	1 months	+ +	+	RCC	Single	Yes	Open/Nep	10	[b]Rec (4 m)	Dead
4	M	39	Hematuria, lower abdominal pain	2 years	+ + +	+ + +	RCC	Single	No	Open/Nep	12	Rec (2 m) Met (4 m)	Dead
5	F	54	None, found incidentally	15 days	+	−	RCC	Single	No	Lap/NSS	9	None	Alive
6	M	37	Left back pain	6 months	−	−	RCC	Single	No	Open/Nep	17	Rec (15 m)	Alive
7	M	82	None, found incidentally	15 days	+ +	−	RCC	Single	No	Open/Nep	7	None	Alive
8	M	48	Hematuria, right back pain	1 months	+ + +	−	RCC	Single	No	Lap/Nep	19	None	Alive
9	F	41	Left back pain	10 days	−	−	RCC	Single	No	Lap/Nep	50	None	Alive
10	M	49	Left back pain	1 months	+	−	RCC	Single	No	Open/Nep	35	None	Alive
11	M	49	Left back pain	15 days	−	−	RCC	Single	No	Open/Nep	8	None	Alive
12	F	20	Right back pain	16 days	+	−	RCC	Single	No	Open/NSS	10	None	Alive

[a]F, female; M, male; Y, years; D, days; M, months; UBC, urine blood occult; UP, urine protein; RCC, renal cell carcinoma; TN, tumor number; Pre-met, preoperative metastatic disease; Lap, laparoscopic; Nep, nephrectomy; NSS, nephron-sparing surgery; Rec, recurrent disease; Met, metastasis
[b]Newly

of them showed an increased distorted appearance (Fig. 1B, F).

Six (50.0%) tumors showed a PE pattern (Fig. 1), two (16.7%) had an EW pattern (Fig. S1), and four (33.3%) showed a GE pattern (Fig. S2, Fig. 2). All tumors appeared with a GW pattern. In addition, a central fibrous scar was found in five (41.7%) patients (Fig. 2), indicating a characteristic persistent enhancement of fibrous tissue. Macroscopic fat was identified in one case (Online Resource 5). "Fast-in, fast-out" nodules were also observed (Fig. 2).

Treatment

All patients received surgery, including laparoscopic nephrectomy (25.0%, 3/12), laparoscopic nephron-sparing surgery (16.7%, 2/12), open nephrectomy (50.0%, 6/12), and open nephron-sparing surgery (8.3%, 1/12). The patient presenting with lung metastasis was recommended to receive further adjuvant radiochemotherapy after palliative resection surgery, but the patient declined. The remaining 11 patients did not receive any adjuvant therapy.

Pathological findings

Macroscopically, the tumors appeared as soft, well-circumscribed ovals ($n = 8$) or irregular ($n = 3$) masses with gray or yellowish-white appearances. Cystic degeneration (8.3%, 1/12) and necrosis (25.0%, 3/12) were observed. Microscopically, the tumors were composed of juxtaposed hyper-cellular and hypo-cellular spindle cell proliferation with a dense collagenous stroma, and various quantities of vascular tissue in a staghorn configuration (Table 3, Fig. 4A–H).

Of the 12 patients, eight (66.7%) patients were classified as having grade I (benign) tumors and the remaining four (33.3%) as having grade III malignant tumors. The malignant tumors (median: 12.57 cm) were significantly larger than the benign ones (median: 3.88 cm) ($P < 0.001$). Although the grade III tumors tended to show higher rates of atypical or malignant features (Fig. 4J-L), these features were identified in all patients (Online Resource 6). Abundant tumor vasculature was observed in both grades of tumors. However, the vessel shapes in the grade I lesions appeared more normal, while the grade III lesions tended to contain distorted blood vessels with an abnormally flattened lumen (Fig. 4C, F, I). In addition, invasion of the renal capsule was found for the grade III lesions (Fig. 4L). IHC analysis was performed, and the details are in Online Resource 6.

Follow-up

All patients had a follow-up clinical visit after discharge. The-time to-follow-up ranged from seven to 82 months, with a mean of 34 months. The details are in Table 1.

Table 2. CT imaging findings for the 12 rSFT/HPCs

Case no.	Location/origin	Size (cm)	CT_{pre} (HU)[a]	Pre-enhanced appearance	Hypo-density[b]	Enhanced appearance	Enhanced pattern	Central scar	OIV	Shape
1	Left upper pole near hilum/parapelvic	2.92	37.55	Slightly hyper	Yes	Slightly hetero	SI-SW	No	No	Slightly lob
2	Left upper pole near hilum/parapelvic	6.49	48.37	Iso/slightly hypo	Yes	Hetero, multiple nodular	SI-SW, fast washout nodule	Yes	Yes	Lob
3	Entire right kidney	9.79	54.04	Iso/slightly hyper with obvious hypo in center region	Yes	Hetero, irregular nodular	GP	No	No	Lob
4	Entire right kidney	12.34	20.29	Mixed hyper/hypo/iso	Yes	Slightly hetero, irregular nodular	GP	No	Yes	Deep lob/multiple nodular
5	Left renal hilum/parapelvic	2.70	31.84	Slightly hyper	Yes	Slightly hetero	GP	No	No	Slightly lob
6	Left renal hilum/parapelvic	12.80	29.33	Mixed hypo/iso (onion-like)	Yes	Hetero	GP	No	Yes	Lob
7	Left middle pole near hilum/parapelvic	16.48	36.21	Slightly hyper with obvious hypo in the center region	Yes	Hetero	GP	No	Yes	Lob
8	Right renal hilum/parapelvic	2.10	42.22	Slightly hyper with slightly hypo in the center region	Yes	Hetero	FI-SO	Yes	Yes	Lob
9	Left renal hilum/parapelvic	6.12	29.73	Slightly hyper with slightly hypo in the center region	No	Hetero	FI-SO	Yes	Yes	Lob
10	Left renal hilum/parapelvic	9.52	45.46	Slightly hyper	Yes	Hetero	GP	Yes	No	Lob
11	Left renal hilum/parapelvic	4.30	34.48	Slightly hyper	Yes	Hetero, multiple nodular	GP	Yes	No	Slightly lob
12	Right renal hilum/parapelvic	3.46	36.45	Slightly hyper	Yes	Homo	FI-SO	No	No	Slightly lob

Boundary/contour	Cal	Hem	Perirenal soft tissue/renal vein invasion	AELN/MET	Hydronephrosis	Fat	PCR	Concomitant disease
Well-defined, blunted	No	No	None	None	No	Yes	No	AML
Well-defined, sharp	No	No	Perirenal fascia	None	Slightly	No	No	None
Ill-defined, blunted	No	No	Perirenal fascia (multiple nodules), ureter	Met	N/A	No	No	None
Ill-defined, blunted	No	Yes	Perirenal fascia (multiple nodules), ureter	Multiple AELN	N/A	No	No	None
Well-defined, sharp	No	No	No	No	No	No	No	None
Regional ill-defined, blunted	No	No	Perirenal fascia	Multiple AELN	Slightly	No	Yes	None
Regional ill-defined, blunted	Yes	No	Perirenal fascia	No	No	No	Yes	None
Regional ill-defined, blunted	No	No	No	No	No	No	No	Multiple AML
Regional ill-defined, blunted	No	No	No	No	Intermediate	No	No	Renal lithiasis
Regional ill-defined, blunted	Yes	No	No	No	Slightly	No	No	None
Well-defined, blunted	No	No	No	No	Slightly	No	No	Renal lithiasis
Well-defined, sharp	No	No	No	No	Slightly	No	No	Renal lithiasis

[a]CT_{pre}, CT value on pre-enhanced images; Hyper, hyperdense; Hypo, hypodense; Iso, isodense; Hetero, heterogeneous; Homo, homogeneous; SI-SO, "slow in, slow out"; GP, gradual progressive; FI-SO, "fast in, slow out"; OIV, obvious intratumoral vessels; Lob, lobulated; Cal, calcification; Hem, hemorrhage; AELN, adjacent enlarged lymph nodes; MET, metastasis; N/A, not applicable; Fat, macroscopic fat; PCR, paratumoral cystic region; AML, angiomyolipoma

[b]Compared to renal parenchyma on enhanced images

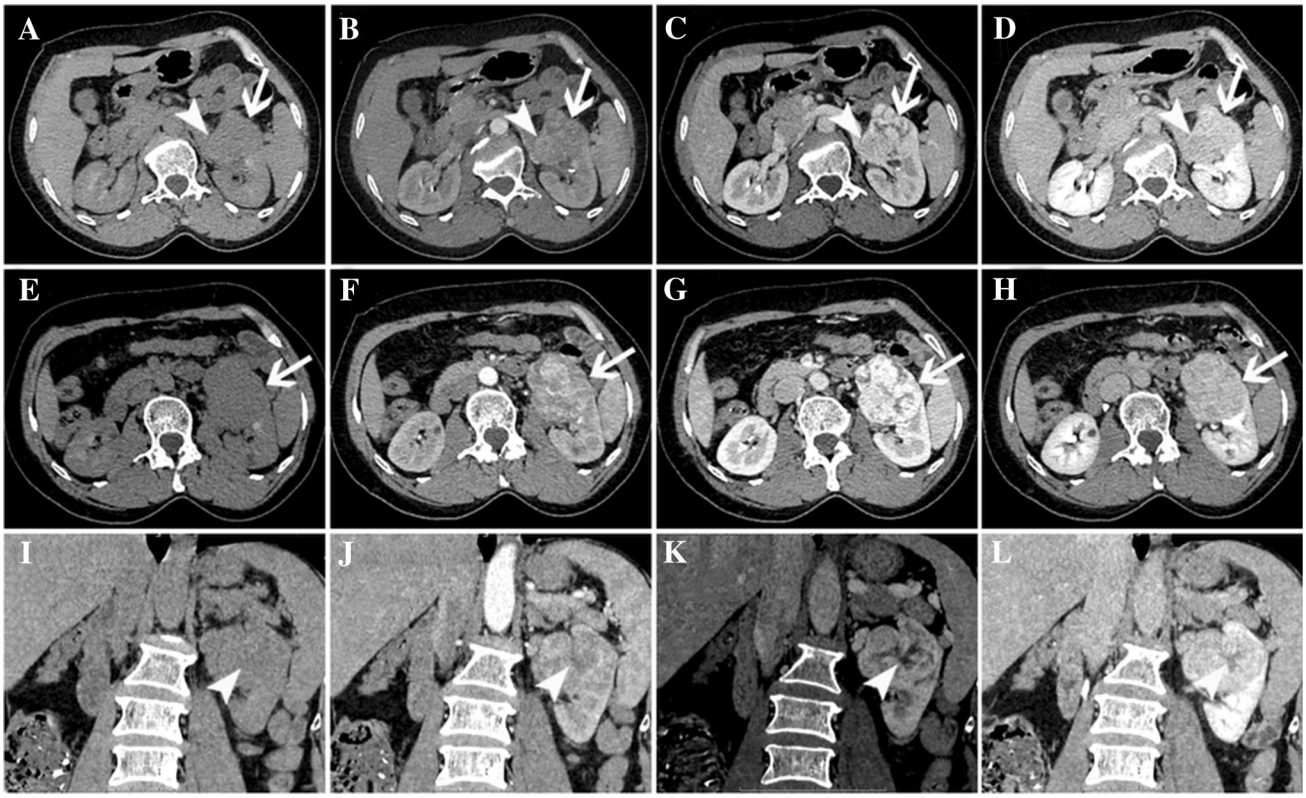

Fig. 2. A 60-year-old female with lower abdominal pain (case 2) presented with rSFT/HPC in the left upper pole kidney near the renal hilum at the parapelvic location (**A**–**D**, arrows). Panels **E**–**H** are three-phase enhanced renal CT images showing a "fast-in, fast-out" enhancing nodule (arrowheads) located in the tumor and a mass (arrows) generally presenting a gradual enhancement (GE) pattern. Panels **I**–**L** (arrowheads) show a central scar sign with shrinking after persistent enhancement.

Discussion

In the present study, we collected a series of 12 rSFT/HPCs to explore characteristic CT imaging features that could improve the pre-operative characterization of this rare tumor. To the best of our knowledge, our study is the first to present imaging features of rSFT/HPCs. Similar to previous reports in the literature [11, 16, 18], we found that rSFT/HPCs occurred predominantly in asymptomatic middle-aged patients. Both men and women were affected equally. Except for the tumors that involved the entire kidney, the rSFT/HPCs in our study cohort were in the renal sinus area, causing only mild-to-moderate hydronephrosis regardless of the size of the tumor.

According to the limited previous literature [5, 16, 19], there is no consensus about the origin of the rSFT/HPCs. In our case series, most of the rSFT/HPCs originated in the renal sinus. Though it has not been clearly stated in previous reports, it is not uncommon to find clues supporting a renal sinus origin for rSFT/HPCs [1, 20, 21]. This is consistent with the studies reporting that rSFT/HPCs originate from the renal capsule [2, 21]. Considering that RCC rarely occurs in the renal sinus, our finding may help clinicians identify renal sinus tumors as rSFT/HPCs; this insight could greatly reduce the scope of diseases listed in the differential diagnosis.

Similar to previous reports, most rSFT/HPCs in our study commonly appeared slightly hyperdense on the unenhanced CT images, appeared somewhat black-and-white, and were surrounded by a pseudocapsule due to hyperdensity on the pre-contrast scan [10, 20]. However, in most cases, the margins of the pseudocapsule were not sharp. In fact, the boundary between the tumor and normal renal parenchyma was usually regionally blunted, whether the tumor was benign or malignant [21]. Interestingly, regardless of the tumor size, none of our patients showed severe obstructive hydronephrosis except for mild-to-moderate hydronephrosis in six patients. We speculate that the lobulated shape, extrarenal exophytic growth pattern, and infiltrative growth pattern may partially represent the "soft" characteristics of rSFT/HPCs. This distinctive CT characteristic can be useful to differentiate rSFT/HPCs from other renal tumors.

Similar to previous reports, all rSFT/HPCs in this study were misdiagnosed as RCCs pre-operatively [15]. Indeed, an EW pattern was identified in two rSFT/

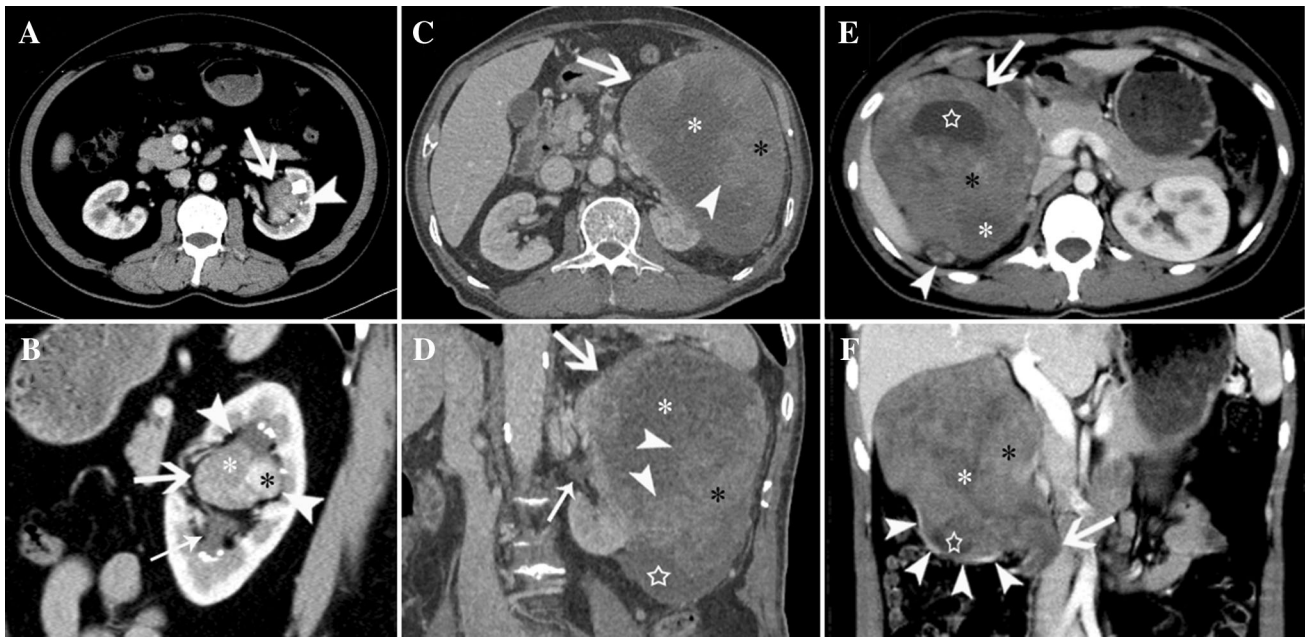

Fig. 3. Three growth patterns of rSFT/HPCs. **A**, **B** A 49-year-old male patient with left back pain (case 11) presented with a mass located in the left renal hilum/parapelvic location. Arrows showing the tumor within the renal pelvis, with a lobulated appearance (arrowheads) with mixed texture. Hypodense (**B**, white asterisks) and hyperdense components (**B**, black asterisks) are visible after enhancement. A thin arrow shows a slightly dilated renal calyx. **C**, **D** An 82-year-old asymptomatic male (case 7) presented with a mass located in the left middle pole of the kidney near the hila/parapelvic location. The tumor (arrows) shows an exophytic growth pattern. After intravenous contrast administration, the tumor shows a mixed appearance with hypodense components (white asterisks), and hyperdense components (black asterisks), forming a papillary shape (arrowhead). Panel **D** shows the paratumoral cystic part (star) and a normal renal pelvis (thin arrow). **E**, **F** A 35-year-old female with right back pain (case 3) presented with a right renal mass involving the entire right kidney. The tumor is shown with an intrarenal infiltrative growth pattern, gross invasion of the renal parenchyma (arrowhead), and cystic degeneration (stars). The heterogeneous mass is shown with hypodense (white asterisks) and hyperdense components (black asterisks). The residual dilated renal pelvis (**E**–**F**, stars), the residual renal parenchyma (**F**, arrowheads), additional tumor nodules in the perinephric fascia next to the tumor (**E**, arrowhead), and the ureter involved by the tumor (**F**, arrow) are shown.

HPCs, which is similar to the hallmark fast-in, fast-out enhancement pattern of RCC. However, 66.7% (8/12) of tumors demonstrated a somewhat progressive enhancement pattern (GE and PE). Therefore, it is not appropriate for all renal tumors to be considered as RCCs preoperatively. We speculate that the key reason for the misdiagnosis was that the renal sinus origin of these tumors was not stressed. It is extremely rare for RCCs [15, 22], to originate from the renal sinus, with an incidence of only 1.2% (3/246) based on data from our hospital (unpublished observation). Some rSFT/HPC findings reported by other researchers [22, 23], such as displacement of renal hilum vessels for reasons other than invasion, may also contribute to differentiating rSFT/HPCs from other hypervascular renal tumors, including RCC.

All rSFT/HPCs in the present study demonstrated a GW pattern. Generally, for a tumor, the type of washout pattern depends on the concentration of tumor cells, distribution/amount of dense collagen fibers, degeneration and tumor necrosis, tumor vessels, and thickness of the vessel wall [1, 2]. Therefore, for rSFT/HPC tumors, the PE pattern (“slow-in, slow-out”) may be due to the abundance of collagen fibers, which may restrict diffusion of contrast agent within the tumor [24, 25]. Although it is difficult to evaluate the fibrous tissue based on the CT images, another typical radiological feature, named the “central scar” sign, was observed in the present study. The central scar sign has not been mentioned for rSFT/HPCs before, and yet was observed in 57.5% (5/8) of the benign rSFT/HPCs (grade I) in our study. Our study findings are supported by Johnson et al. [26], who reported a case with areas of very low signal intensity throughout the mass on T2-weighted HASTE images; they attributed the low intensity to dense collagenization and fibrosis.

Malignant rSFT/HPCs are usually characterized by aggressive clinical behavior and account for 10-20% of all rSFT/HPCs. It is important but challenging for clinicians to distinguish between benign and malignant rSFT/HPCs [12]. As demonstrated in this study, there are several differences in the CT features between benign and

Table 3. Pathological findings for the 12 rSFT/HPCs

Case no.	Grade	Vimentin levels	CD34 levels	CD99 levels	BCL-2 levels	Ki-67 levels	S-100 levels	Epithelial membrane antigen levels	Nuclear atypia	Cellular pleomorphism	Hyper-cellularity	High mitotic rate (> 4 mitoses/10 high-power fields)	Necrosis
1	I	+	A few cells only +	+	+	< 2%	–	A few cells only +	+	+	Focally +	+	–
2	I	+	+	+	+	< 2%	–	–	–	Focally +	+	–	–
3	III	+	Scattered Focally +	A few cells only +	Weakly +	5% +	–	–	–	+	Focally +	+	+
4	III	+	Focally +	Focally +	+	15%	–	–	+	+	+	+	–
5	I	A few cells only +	+	+	+	5% +	–	–	–	–	–	–	–
6	III	+	A few cells only +	+	Weakly +	50% +	–	–	+	+	+	+	+
7	III	+	Strongly +	Focally +	Weakly +	40% +	–	A few cells only +	+	+	+	+	+
8	I	A few cells only +	+	+	–	5% +	–	–	–	–	–	–	–
9	I	Weakly +	+	+	–	3%	–	–	–	–	Focally +	–	+
10	I	+	A few cells only +	Focally +	Weakly +	8%	–	–	Dubious +	Dubious +	+	–	–
11	I	A few cells only +	–	+	Focally +	< 2%	–	–	–	–	Focally +	–	–
12	I	Focally +	Weakly +	Focally +	Focally +	3%	–	–	–	Focally +	Focally +	–	–

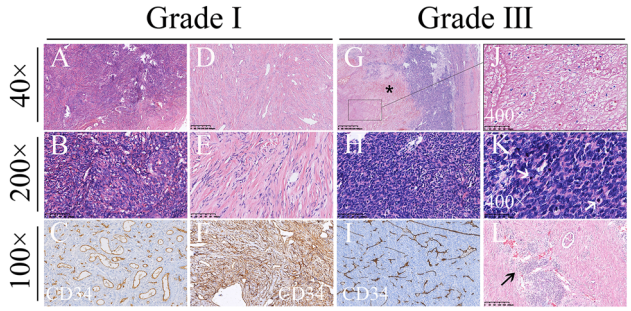

Fig. 4. Pathological findings in patients with rSFT/HPCs (**A–C**, case 1; **D–F**, case 5; **G–L**, case 6). (**A–B**, **D–E**, **G–H**) Hematoxylin/eosin staining showing juxtaposed hyper- and hypo-cellular spindle cell proliferation, dense collagenous stroma, and various quantities of vascular tissue with a staghorn configuration. (**C**, **F**, **I**) CD34 staining shows the intratumoral vasculature. With increasing tumor grade (grade I–III), the proportion of distorted/twisted vessels increased, and the corresponding vascular lumen was narrowed, especially in areas with dense tumor cells in the grade III tumor (**I**). Panels **G** and **J** (magnification of the rectangular area in G) show multiple diffusely distributed necrotic areas accompanied by hemorrhage. Mitotic counts (**K**, arrow) and capsule invasion (**L**, arrow) are also shown.

malignant rSFT/HPCs. Compared with benign rSFT/HPC (grade I) lesions, the malignant rSFT/HPC (grade III) lesions tend to be larger with a maximal diameter over 10 cm, and to appear more heterogeneous. In addition, the malignant legions show a PE pattern with a higher rate of renal fascia invasion. Furthermore, malignant rSFT/HPCs have enlarged intratumoral vessels, a higher rate of enlarged regional lymph nodes, a higher rate of paratumoral cystic regions, and a lower rate of the central scar sign. Additionally, proteinuria was only present in two grade III patients. Tumors tend to be larger with increasing grade (from I to III), as shown in literature reviews in the Online Resource 1. Interestingly, we found that distorted intratumoral vessels with narrowed lumen were common in malignant rSFT masses but not in benign rSFT/HPC lesions. This morphological changes in the blood vessels might be due to the compression of tumor cells. It is plausible to speculate that there would be subsequent hemodynamic changes in the vessels and contrast medium diffusion would be restricted. This would cause contrast agent to enter and exit the tumor gradually, which may partially explain why a slowly enhanced pattern (PE or GW pattern) was identified in the malignant tumors.

Differential diagnosis mainly includes tumors located around the renal hilum, especially those originating from the renal sinus [27], such as another mesenchymal tumor, RCC protruding into the renal sinus, retroperitoneal tumor invasion, and renal sinus metastatic tumor. However, in most instances, a definitive tumor location in the renal sinus could exclude the possibility of a renal

parenchymal tumor or a retroperitoneal tumor. Some other mesenchymal tumors in the renal sinus can be differentiated from rSFT/HPCs because of their typical radiological characteristics. For example, lipomas and angiomyolipomas may have macroscopic fat and Castleman disease may have characteristic arborizing calcification [7, 27]. Although the fat-forming rSFT/HPCs may be confusing, they are rare and there have only been three such cases reported [11]. Paragangliomas usually present as a mass with avid contrast enhancement and delayed wash-out along with cystic changes, necrosis, and internal calcifications [28]. It might be challenging to differentiate rSFT/HPCs from other mesenchymal tumors located in renal sinus, such as leiomyoma, leiomyosarcoma, liposarcoma, non-Hodgkin's lymphoma, and paragangliomas, due to potentially overlapping imaging features [7]. Nevertheless, the imaging characteristics of rSFT/HPCs identified in the present study may improve the differential diagnosis.

There are several limitations in the present study. First, the number of patients in our study was modest, although it is the largest collection of such patients reported to the best of our knowledge. Our imaging findings may need to be validated in future studies with a larger sample size. Second, the lack of grade II tumors in our case series may have affected the reproducibility of our findings. Third, the underlying pathological basis for the imaging findings was not clear. A multicenter prospective study with radiological and pathological correlation might be necessary to understand the pathological basis for the imaging findings. Last, our study was limited by a lack of magnetic resonance imaging (MRI) features. MRI of the kidneys might be helpful to further characterize the rSFT/HPCs, given its multiplanar multisequence capability and lack of radiation risk.

Our results suggest that rSFT/HPCs usually arise from the renal sinus. These rare renal tumors may have a slightly hyperdense pseudocapsule around the tumor on unenhanced CT images. In addition, most rSFT/HPCs have a PE pattern rather than the fast-in and fast-out enhancement pattern of RCC. The rSFT/HPCs may displace the renal hilar vessels, unlike RCC, which replaces them. Furthermore, the large tumor size, PE pattern, regional lymph node involvement and lack of a central scar should suggest malignant rSFT/HPC.

Conclusions

In summary, rSFT/HPCs tend to present as a lobulated, slightly hyperdense, progressively enhancing masses arising from the renal sinus. The presence of a central scar may indicate a benign (grade I) tumor. If a large, heterogeneous mass originating in the renal sinus ($>$ 10 cm maximal diameter) has a PE pattern, malignant rSFT/HPC should be considered.

Acknowledgements We thank Taihao Jin (Ph.D.) from City of Hope National Medical Center for helpful discussion. We also thank doctors Hongling Yin and Desheng Xiao from the Department of Pathology (Xiangya Hospital, Central South University) for the detailed pathological analysis. Nancy Linford, PhD, provided editing assistance.

Author contributions YXP, ZYM conceived and designed the study. YXP, WJ, WZX, ZZN, GGH, ZYM analyzed the data. YXP, WJ, WZX, ZZN, LWH, ZYM, CBH contributed to data analysis. YXP, WJ, WZX, ZYM, ZCS, CBH prepared the paper. All authors read and approved the final version of the manuscript.

Compliance with ethical standards

Funding This study was supported in part by The Postdoctoral Science Foundation of Central South University (Grant Number 185705).

Conflict of interest The authors declare that they have no conflict of interest.

Ethical approval All procedures performed in studies involving human participants were in accordance with the ethical standards of the institutional and/or national research committee and with the 1964 Helsinki declaration and its later amendments or comparable ethical standards. For this type of study formal consent is not required.

References

1. Louis DN, Perry A, Reifenberger G, et al. (2016) The 2016 World Health Organization classification of tumors of the central nervous system: a summary. Acta Neuropathol 131:803–820. https://doi.org/10.1007/s00401-016-1545-1
2. Sahm F, Reuss DE, Giannini C (2017) WHO 2016 Classification: changes and advancements in the diagnosis of miscellaneous primary CNS tumours. Neuropathol Appl Neurobiol . https://doi.org/10.1111/nan.12397
3. Macagno N, Figarella-Branger D, Mokthari K, et al. (2016) Differential diagnosis of meningeal SFT-HPC and meningioma: which immunohistochemical markers should be used. Am J Surg Pathol 40:270–278. https://doi.org/10.1097/PAS.0000000000000526
4. Zhou Y, Chu X, Yi Y, Tong L, Dai Y (2017) Malignant solitary fibrous tumor in retroperitoneum: a case report and literature review. Medicine (Baltimore) 96:e6373. https://doi.org/10.1097/MD.0000000000006373
5. Jiang N, Xie YY, Chen W, et al. (2017) Solitary fibrous tumor of central nervous system: clinical and prognostic study of 24 cases. World Neurosurg 99:584–592. https://doi.org/10.1016/j.wneu.2016.12.057
6. Yi X, Xiao D, He Y, et al. (2017) Spinal solitary fibrous tumor/hemangiopericytoma: a clinicopathologic and radiologic analysis of eleven cases. World Neurosurg 104:318–329. https://doi.org/10.1016/j.wneu.2017.05.016
7. Sasaguri K, Takahashi N (2018) CT and MR imaging for solid renal mass characterization. Eur J Radiol 99:40–54. https://doi.org/10.1016/j.ejrad.2017.12.008
8. Karaosmanoğlu AD, Onur MR, Shirkhoda A, Ozmen M, Hahn PF (2015) Unusual benign solid neoplasms of the kidney: cross-sectional imaging findings. Diagn Interv Radiol 21:376–381. https://doi.org/10.5152/dir.2015.14545
9. Raman SP, Hruban RH, Fishman EK (2012) Beyond renal cell carcinoma: rare and unusual renal masses. Abdom Imaging 37:873–884. https://doi.org/10.1007/s00261-012-9903-5
10. Wu WW, Chu JT, Romansky SG, Shane L (2015) Pediatric renal solitary fibrous tumor: report of a rare case and review of the literature. Int J Surg Pathol 23:34–47. https://doi.org/10.1177/1066896913492847
11. Chen Y, Wang F, Han A (2015) Fat-forming solitary fibrous tumor of the kidney: a case report and literature review. Int J Clin Exp Pathol 8:8632–8635
12. Yang Y, Miller CR, Clement C, Hes O, Eyzaguirre E (2017) Malignant solitary fibrous tumour of the kidney with lymph node and liver metastases. Pathology 49:450–453. https://doi.org/10.1016/j.pathol.2017.01.014

13. Liu L, Qi L, Li Y, et al. (2017) Retroperitoneoscopic partial nephrectomy for moderately complex ventral hilar tumors: surgical technique and trifecta outcomes from a single Institution in China. J Laparoendosc Adv Surg Tech A 27:812–817. https://doi.org/10.1089/lap.2016.0194
14. Liu W, Li Y, Chen M, et al. (2014) Off-clamp versus complete hilar control partial nephrectomy for renal cell carcinoma: a systematic review and meta-analysis. J Endourol 28:567–576. https://doi.org/10.1089/end.2013.0562
15. Tsivian M, del Pilar Laguna Pes M, Rampersaud EN, et al. (2014) Small renal mass biopsy–how, what and when: report from an international consensus panel. BJU Int 113:854–863. https://doi.org/10.1111/bju.12470
16. Wood CG, Stromberg LJ, Harmath CB, et al. (2015) CT and MR imaging for evaluation of cystic renal lesions and diseases. Radiographics 35:125–141. https://doi.org/10.1148/rg.351130016
17. Millet I, Doyon FC, Hoa D, et al. (2011) Characterization of small solid renal lesions: can benign and malignant tumors be differentiated with CT. AJR Am J Roentgenol 197:887–896. https://doi.org/10.2214/AJR.10.6276
18. Bezerra ES, Andrighetto OP, Costa MV, et al. (2018) Bilateral renal involvement by solitary fibrous tumor—Report of a case in the post-WHO/2016 era. Urol Case Rep 17:7–9. https://doi.org/10.1016/j.eucr.2017.12.003
19. Ichiyanagi O, Ito H, Takai S, et al. (2015) A GRIA2 and PAX8-positive renal solitary fibrous tumor with NAB2-STAT6 gene fusion. Diagn Pathol 10:155. https://doi.org/10.1186/s13000-015-0386-x
20. Tritschler P, Coulier B, Gielen I (2014) Solitary fibrous tumor of the kidney. JBR-BTR 97:298–300
21. Park SB, Park YS, Kim JK, et al. (2011) Solitary fibrous tumor of the genitourinary tract. AJR Am J Roentgenol 196:W132–137. https://doi.org/10.2214/AJR.09.3787
22. Delahunt B, Srigley JR, Montironi R, Egevad L (2014) Advances in renal neoplasia: recommendations from the 2012 International Society of Urological Pathology Consensus Conference. Urology 83:969–974. https://doi.org/10.1016/j.urology.2014.02.004
23. Hayasaka K, Nihashi T, Nojiri Y, Okamuara K (2007) Computed tomography manifestations of renal hemangiopericytoma. Acta Radiol 48:934–937. https://doi.org/10.1080/02841850701459767
24. Amano T, Suzuki SO, Mizoguchi M, et al. (2013) Fibrotic nodule arising from the cerebellopontine angle. Brain Tumor Pathol 30:122–127. https://doi.org/10.1007/s10014-012-0105-1
25. Galateau-Salle F, Churg A, Roggli V, Travis WD (2016) The 2015 World Health Organization classification of tumors of the pleura: advances since the 2004 classification. J Thorac Oncol 11:142–154. https://doi.org/10.1016/j.jtho.2015.11.005
26. Johnson TR, Pedrosa I, Goldsmith J, Dewolf WC, Rofsky NM (2005) Magnetic resonance imaging findings in solitary fibrous tumor of the kidney. J Comput Assist Tomogr 29:481–483
27. Young A, Kunju LP (2012) High-grade carcinomas involving the renal sinus: report of a case and review of the differential diagnosis and immunohistochemical expression. Arch Pathol Lab Med 136:907–910. https://doi.org/10.5858/arpa.2012-0196-CR
28. Liu HW, Liu LR, Cao DH, Wei Q (2014) Paraganglioma in the renal pelvis. Kaohsiung J Med Sci 30:319–320. https://doi.org/10.1016/j.kjms.2013.04.007